

Coupling a Fabry–Pérot Cavity to a Single-Mode Optical Fiber Using a Metalens

Wance Wang

Department of Physics, University of Maryland, College Park, Maryland, USA

Wenqi Zhu

Physical Measurement Laboratory, National Institute of Standards and Technology, Gaithersburg, MD, USA

Amit Agrawal

Department of Engineering, University of Cambridge, Cambridge, UK

Joseph W. Britton

*Department of Physics, University of Maryland, College Park, Maryland, USA and
DEVCOM Army Research Laboratory, Adelphi, MD, USA*

Efficient coupling of light from an optical cavity to a single-mode fiber is required in a range of quantum technologies. In this work we consider the coupling of a high-finesse macroscopic Fabry–Pérot (FP) cavity to a single-mode fiber using a metalens. We perform sensitivity analysis with respect to longitudinal and transverse misalignment errors. We then detail a fiber-coupled cavity at 1650 nm using a monolithic cryo-compatible assembly incorporating a metalens.

I. INTRODUCTION

Photon collection enables qubit readout and fluorescence imaging in a variety of quantum platforms including neutral atoms [1–3], trapped ions [4–6], color centers [7] and quantum dots [8]. These systems can also generate single photons, a critical resource for quantum networking [9–12]. High-NA free-space optics permit impressive collection efficiency from point emitters (up to $4\pi \times 0.3$ sr [1]) but rely on very complex optical assemblies. An alternative approach places the emitter in an optical cavity that enhances photon emission into a well-defined spatial mode via the Purcell effect [10, 13, 14], but shifts complexity from refractive optics to arguably more complex in-vacuum alignment-sensitive optical cavities. The optimization of populating a cavity mode by an atom-generated photon is well studied [15–17]. The related problem of efficiently coupling the cavity to a single-mode (SM) optical fiber also requires careful analysis.

The leading approaches to build in-vacuum Fabry–Pérot (FP) cavities rely on mirrors formed on fiber tips [18] or macroscopic formed-glass mirrors [19, 20]. For fiber-cavities, mode matching has been explored in depth [18, 21–23]. And, up to 90% coupling efficiency was demonstrated using graded index (GRIN) fiber elements [24]. However, this technique is not readily transferable to macroscopic cavities as it relies on fiber fusion-splicing. We extend the range of techniques for in-vacuum fiber coupling of macroscopic mirrors by exploring the use of metamaterial-based lenses.

Metalenses [25] are two-dimensional engineered nanostructures that manipulate the phase of light similar to a refractive optic but are vanishingly thin and quite versatile. For example, 0.9 NA metalenses have been demonstrated with diffraction efficiency of 0.89 and total efficiency (including reflection and absorption) of 0.67[26]. In AMO physics, metalenses have been successfully used to trap neutral atoms [27–29], collect fluorescence from an atom [30], generate orbital angular momentum light field [31, 32], and form an FP cavity

[33]. These designs have successfully reduced the footprint and enhanced the mechanical robustness in their respective applications.

In this manuscript we explore coupling of a macroscopic FP cavity to an SM optical fiber using a metalens. We work with a geometry where one cavity mirror is free-space coupled and the other is fiber coupled. In this context we analyze the sensitivity of fiber-cavity coupling efficiency to a variety of misalignment errors. We then build a monolithic assembly to couple the TEM00 mode of a FP cavity at 1650 nm into a telecom SM fiber using a metalens. Finally, we discuss the tradeoffs of using metamaterials for beam forming in the context of single-photon experiments.

II. GEOMETRIC ALIGNMENT TOLERANCE

The conventional approach is to put the cavity in-vacuum along with non-adjustable refractive collimating optics [5]. The collimated beam then passes thru a vacuum window and is fiber-coupled using an asphere. Such spatially extended beam lines are sensitive to vibration and drift—especially in cryogenic setups [34–36]. Here, we aim to extend the range of cavity-fiber coupling options by exploring a compact in-vacuum assembly with the fiber tip and fiber mode matching optics positioned close to the cavity. We present our design below and carry out a tolerance analysis to guide fabrication and use of the assembly.

The goal of our optical assembly is to mode match a cavity TEM00 mode to a single-mode fiber mode using a metalens. Our design of the assembly is illustrated in Fig. 1(a). The cavity has a length d , mirror radius of curvature R and mirror thickness d_t . The mirrors are mirror symmetric about the cavity waist (radius w_c). The cavity mode is propagagted to the fiber tip by the metalens (focal length f) at a position d_s with a waist w_s . An SM fiber (core mode field diameter $2w_f$) is mechanically integrated with the left cavity mirror using a holder.

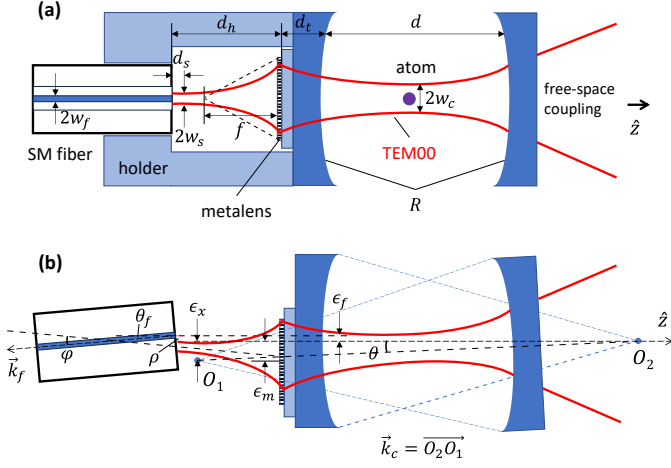


FIG. 1. Cross section of the optical assembly consisting of a pair of mirrors forming a FP cavity, a metalens and a SM fiber. (a) A diagram showing how longitudinal alignment errors can produce a beam waist w_s different from the fiber w_f at a position d_s away from the fiber tip. A mechanical holder for the fiber is also shown. (b) A diagram showing transverse alignment errors.

The distance from the metalens to the fiber tip is d_h .

We now vary f and d_h to maximize the coupling. The cavity TEM00 mode waist is

$$w_c = \sqrt{\frac{\lambda}{\pi}} \left[\frac{d(2R-d)}{4} \right]^{1/4} \quad (1)$$

The metalens lies distance $d_o = d/2 + d_t$ from the cavity waist. The lens equation is

$$\frac{1}{d_o + z_R^2/(d_o - f)} + \frac{1}{d_h - d_s} = \frac{1}{f} \quad (2)$$

$z_R = \pi w_c^2/\lambda$ is the Rayleigh range. The transformed beam waist is

$$w_s = \frac{1}{\sqrt{(1 - d_o/f)^2 + (z_R/f)^2}} w_c \quad (3)$$

. Ideal coupling is obtained by solving for f and d_h so that $d_s = 0$ and $w_s = w_f$.

Two cavity geometries To achieve high cooperativity with atomic quantum emitters, a small cavity waist is desired [37–41]. Here we consider two example cavity geometries: one stable and one near-concentric.

1. $R = 50$ mm, $d = 10$ mm: $w_c = 86$ μm , $f = 1.056$ mm, $d_h = 1.088$ mm. Stability parameter $g_1 g_2 = (1 - d/R)^2 = 0.64$.
2. $R = 5$ mm, $d = 9.98$ mm (near-concentric): $w_c = 10$ μm , $f = 3.310$ mm, $d_h = 4.949$ mm. Stability parameter $g_1 g_2 = (1 - d/R)^2 = 0.99$.

In both cases we assume $d_t = 5$ mm, $\lambda = 1550$ nm and $2w_f = 10.4$ μm (typical for telecom fiber [42]).

A. Misalignment

We identify errors that give rise to longitudinal and transverse deviations that reduce fiber-cavity coupling. We then perform sensitivity analysis to identify the most critical parameters.

1. Longitudinal misalignment

In this section we evaluate the sensitivity factor of various longitudinal errors then calculate their impact on cavity-fiber coupling. Longitudinal error includes variation in cavity length d , mirror thickness d_t , length d_h , and focal length f . The result of all these errors is a longitudinal shift of the transformed d_s and waist size w_s .

Doing the derivatives, we get the following sensitivities of d_s and w_s .

$$\begin{aligned} \frac{\partial d_s}{\partial d} &= \frac{2f^2(d_t - f)(R + d_t - f)}{[dR + 2(d_t - f)(d + d_t - f)]^2} \\ \frac{\partial d_s}{\partial d_t} &= \frac{2f^2[-dR + (d_t - f)^2 + (d + d_t - f)^2]}{[dR + 2(d_t - f)(d + d_t - f)]^2} \\ \frac{\partial d_s}{\partial d_h} &= 1 \\ \frac{\partial d_s}{\partial f} &= -\frac{d^2[(R + 2d_t - f)^2 + f^2] + 2dR[2d_t(d_t - f) - f^2] + 4d_t(d_t - f)[dd_t + (d + d_t)(d_t - f)]}{[dR + 2(d_t - f)(d + d_t - f)]^2} \end{aligned} \quad (4)$$

$$\begin{aligned}
\frac{\partial w_s}{\partial d} &= -\frac{dR^2 + 2dR(d_t - f) - 2(R - d)(d_t - f)^2}{4d(2R - d)f^2} \left(\frac{w_f}{w_c}\right)^2 w_f \\
\frac{\partial w_s}{\partial d_t} &= -\frac{d + 2d_t - 2f}{2f^2} \left(\frac{w_f}{w_c}\right)^2 w_f \\
\frac{\partial w_s}{\partial d_h} &= 0 \\
\frac{\partial w_s}{\partial f} &= \frac{1}{f} w_f + \frac{d + 2d_t - 2f}{2f^2} \left(\frac{w_f}{w_c}\right)^2 w_f
\end{aligned} \tag{5}$$

Given error Δd , for example, the refracted beam deviation is $\Delta d_s = \frac{\partial d_s}{\partial d} \Delta d$ and $\Delta w_s = \frac{\partial w_s}{\partial d} \Delta d$.

The cavity-fiber coupling can be calculated from an overlap integral between their mode shapes. We assume both are normalized Gaussians. Recall that a Gaussian with waist w_0 located at $z = 0$ has the form

$$E(x, y, z) = \frac{2}{\pi} \frac{1}{w(z)} \exp\left(-\frac{x^2 + y^2}{w(z)^2} - ik\left(z + \frac{x^2 + y^2}{2R(z)} - \psi(z)\right)\right) \tag{6}$$

with beam radius $w(z) = w_0 \sqrt{1 + (z/z_R)^2}$, radius of curvature $R(z) = z \left[1 + (z_R/z)^2\right]$ and Gouy phase $\psi(z)$. Here, the Rayleigh range is $z_R = \frac{1}{2} k w_0^2$ and $k = 2\pi/\lambda$. The overlap integral is

$$\eta = \left| \int_{-\infty}^{\infty} \int_{-\infty}^{\infty} E_s(x, y, 0) E_f^*(x, y, 0) dx dy \right|^2 \tag{7}$$

E_s is the cavity TEM00 Gaussian mode imaged by the metalens and E_f is the Gaussian mode with a waist at the fiber tip (assume the fiber tip at $z = 0$). Waist $w_0 = w_s$ for E_s and $w_0 = w_f$ for E_f .

Ref. [43] relates errors $d_s + \Delta d_s$ and $w_s + \Delta w_s$ to efficiency.

$$\eta_L(\Delta d_s, \Delta w_s) = \frac{4}{\left(\frac{w_s + \Delta w_s}{w_f} + \frac{w_f}{w_s + \Delta w_s}\right)^2 + \left[\frac{2}{k(w_s + \Delta w_s)w_f}\right]^2 (\Delta d_s)^2} \tag{8}$$

Given $w_s = w_f$ and $d_s = 0$, $\eta_L(0, 0) = 1$. Any longitudinal misalignment $p \in \{d, d_t, d_h, f\}$ results in coupling efficiency $\eta_L\left(\frac{\partial d_s}{\partial p} \Delta p, \frac{\partial w_s}{\partial p} \Delta p\right)^1$ (Fig. 2).

For the near-concentric cavity efficiency drops to 50% when any one of the following errors occurs: $\Delta d = 100 \mu\text{m}$, $\Delta d_t = 420 \mu\text{m}$, $\Delta d_h = 110 \mu\text{m}$, or $\Delta f = 50 \mu\text{m}$. Let's check some routine uses cases. When aligning the cavity it's routine to scan the cavity length by 2 free spectral ranges (FSR) to check cavity spectrum, which corresponds to $\Delta d = 2\lambda = 3.1 \mu\text{m} \ll 100 \mu\text{m}$. For the fused silica mirror and holder, it will not expand or contract by $\Delta d_t/d_t$ and $\Delta d_h/d_h$ given any reasonable temperature change. For a metalens manufactured by electron-beam lithography, the focal length error is approximately $1 \mu\text{m}$. Cavity 1 can tolerate much larger longitudinal error. Diffraction and clipping loss are no problem as the metalens diameter is much larger than the beam diameter at $d/2 + d_t$.

2. Transverse misalignment

Transverse errors cause optical path deviations relative to the \hat{z} optical axis. We define \hat{z} as the axis passing through the center of left mirror's circular substrate and the center of curvature O_2 of the left mirror (see Fig. 1(b)). First, if the center of curvature O_1 of the right mirror is transversely displaced from \hat{z} by ϵ_x , the resulting cavity axis $\vec{k}_c = \overrightarrow{O_2 O_1}$ forms an angle θ with \hat{z} . Second, the metalens axis could be offset by ϵ_m relative to the center of the left mirror. Finally, the fiber axis could be tilted by angle θ_f relative to \hat{z} or displaced by an offset ϵ_f left mirror. All sources of transverse misalignment lead to a tilted image at the fiber offset by ρ relative to the fiber core and angle φ relative to the fiber axis \vec{k}_f . Note that in our geometry ρ and φ are dependent variables, that is, they are not independently adjusted.

Using ray transfer matrix analysis, we calculate the sensitivities of ρ and φ to transverse errors ϵ_x , ϵ_m , θ_f and ϵ_f . We consider the worst case scenario where all errors are additive. In this case,

$$\begin{pmatrix} \rho \\ \varphi \end{pmatrix} = \frac{1}{2R - d} \begin{pmatrix} (R + d_t)(1 - \frac{d_s}{f}) + d_s \\ \frac{f - R - d_t}{f} \end{pmatrix} \epsilon_x + \begin{pmatrix} 1 - \frac{d_s}{f} \\ -\frac{1}{f} \end{pmatrix} \epsilon_m + \begin{pmatrix} 0 \\ 1 \end{pmatrix} \theta_f + \begin{pmatrix} 1 \\ 0 \end{pmatrix} \epsilon_f \tag{9}$$

¹ For cavity geometry 2, we change cavity length d to $d - \Delta d$ to avoid push-

ing the cavity to instability.

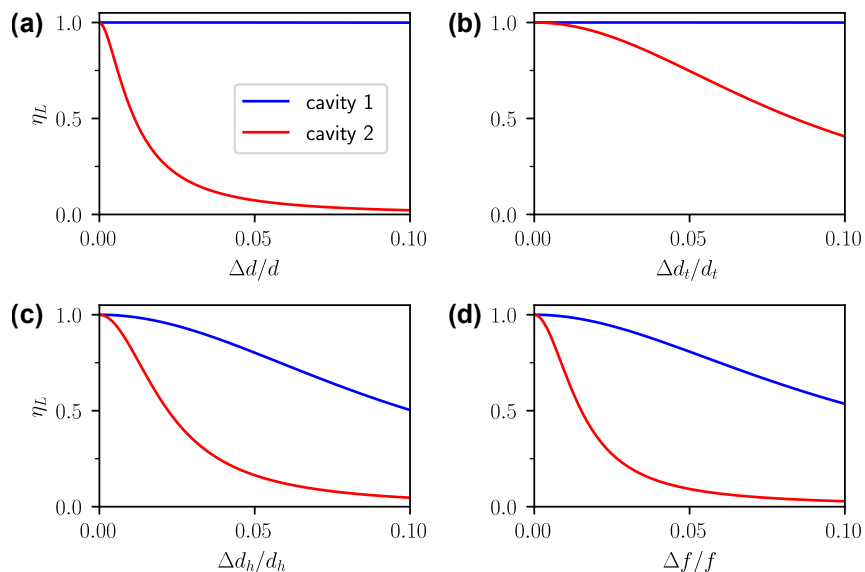


FIG. 2. (a-d) Coupling efficiency η_L a function of Δd , Δd_t , Δd_h , and Δf of the two cavity geometries. Values of d, d_t, d_h, f for the two geometries are listed in II.

The angle between \vec{k}_c and \hat{z} is $\theta = \varepsilon_x / (2R - d)$. We parameterize mirror-mirror misalignment in terms of ε_x as it includes the $2R - d$ geometric factor.

Similarly, assuming no longitudinal error we calculate the efficiency as a function of ρ and φ based on Ref. [43],

$$\eta_T(\rho, \varphi) = \exp \left[-(\rho/w_f)^2 - (\varphi k w_f)^2 \right] \quad (10)$$

. Any transverse misalignment $p \in \{\varepsilon_x, \varepsilon_m, \theta_f, \varepsilon_f\}$ results in a reduced efficiency $\eta_T \left(\frac{\partial \rho}{\partial p} \Delta p, \frac{\partial \varphi}{\partial p} \Delta p \right)$ (see Fig 3).

For the near-concentric cavity (cavity 2) the efficiency drops to 50% when any one of the following errors occurs: $\varepsilon_x = 0.4 \mu\text{m}$ (corresponds to $\theta = 1.1$ deg), $\varepsilon_m = 8.5 \mu\text{m}$, $\theta_f = 2.2$ deg, or $\varepsilon_f = 50 \mu\text{m}$. The transverse errors ε_x and ε_m are particularly consequential to coupling. The tight constraint on ε_x is an inherent challenge of near-concentric cavities. If the mechanical assembly permits tuning of θ_f and offset ε_f , they can be used to compensate for errors in ε_x and ε_m . In contrast, the stable cavity (cavity 1) is much more robust to errors. ¶

III. EXPERIMENTAL SETUP

In this section we describe a monolithic optical assembly that combines mirror, metalens, spacers, fiber and fiber mechanical support. It also details alignment of the assembly in the context of an FP cavity and our characterization of its coupling. We choose a particular cavity geometry based on our atomic system and the constraints of a preexisting ion trap. It closely resembles geometry 1.

Our cavity geometry has $R = 50$ mm and $d = 13$ mm, with optical coatings yielding a finesse of $\sim 20,000$ at 1650 nm,

similar to stable cavity geometry 1. We calculate that for optimal mode matching $f = 1.161$ mm and $d_h = 1.196$ mm.

The metalens for this experiment is constructed from $1.2 \mu\text{m}$ -tall polycrystalline Si nanopillars ($n = 3.47$) patterned by electron beam lithography and fluorine-based reactive ion etch. The nanopillar array is fabricated on a $500 \mu\text{m}$ -thick fused-silica substrate ($n = 1.44$) which is bonded to the AR-coated cavity mirror using UV-cured Norland NOA-61 ($n = 1.54$) [44]. The metalens is designed for a convex focal length of $f = 1.16$ mm at 1650 nm. At this wavelength the metalens transmission is 0.92 and the focusing efficiency is 0.61^2 .

Figure 4(a) illustrates the assembly steps. To mode match the TEM₀₀ mode, the cavity must be well-defined and aligned. In step (1), two optical mounts were aligned to a laser beam by maximizing the transmitted power through two irises so the two mounts are simultaneously concentric and perpendicular to the beam. Cavity mirrors were installed in step (2) and we fine tuned one of the mounts to align the cavity to the beam. In step (3), the left mirror was uninstalled and placed horizontally under a stereoscope. The metalens substrate was panned while visually checking its concentricity relative to the mirror peripheral. We applied an optically transparent epoxy A [44, 46] between the metalens substrate and the mirror. The metalens was adjusted to its final position and then fixed in place by UV curing the epoxy. In step (4), we tuned fiber angle θ_f and offset ε_f to compensate any offset ε_m introduced in step (3). The fiber, mounted in a ferrule, was held in a

² The fraction of light focused to a spot by the meta lens is called the focusing efficiency; the balance of light passes straight thru the metalens. With optimization, the focusing efficiency can be 0.90[26, 45] and may improve over time as metalens design and fabrication improves.

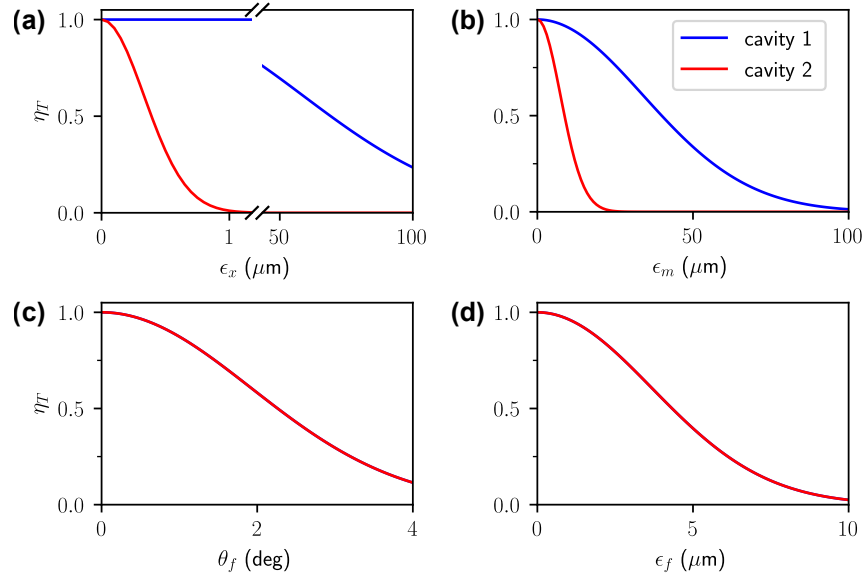


FIG. 3. (a-d) Coupling efficiency η_T a function of ϵ_x , ϵ_m , θ_f , and ϵ_f of the two cavity geometries. In (c,d), traces of two cavities overlap.

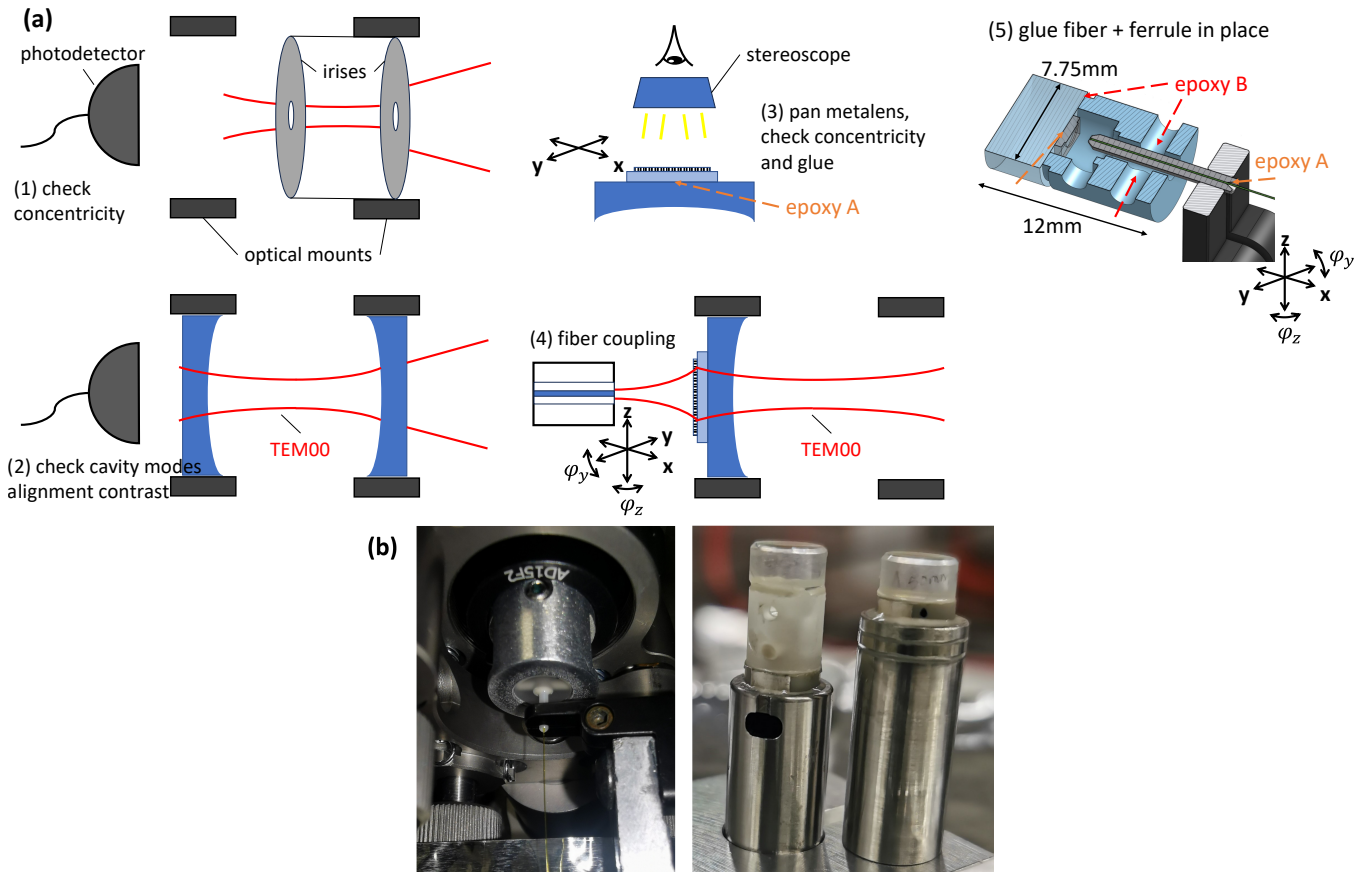


FIG. 4. (a) Illustration of the cavity-fiber integration steps. (b) Left photo: gluing fiber in a ferrule to the holder. Right photo: the finished assembly; left one is the cavity-metalens-fiber assembly (the fiber extends below the metal jig), and the right one is the free-space cavity mirror. They are both glued to metal tube mounts.

stage with 5 degrees of freedom. Here, the left mirror was re-installed and the right mirror was removed. We adjusted the fiber to couple the transmitted light. Finally, in step (5), we glued the holder to the outer rim of the left mirror. The fiber was repositioned to maximize coupling, and the ferrule was fixed in place by potting it inside the holder with epoxy B [44, 47]. The assembly formed a monolithic part after epoxy curing.

During the assembly process we performed several diagnostic measurements. In step (2), we scanned the laser frequency across the full cavity FSR and observed a contrast ratio $> 40 : 1$ between TEM₀₀ and higher-order transverse modes. This confirmed that the input beam closely approximated the TEM₀₀, allowing us in step (4) to use it for fiber coupling without tuning the laser to cavity resonance. We also verified that uninstalling and re-installing the mirrors did not degrade alignment. In step (3), we constrain $\varepsilon_m < 200 \mu\text{m}$ (1/10 of the metalens diameter). Although this accuracy is poor, we compensate in step (4) by tuning θ_f and ε_f . We achieved a relative fiber coupling efficiency of 94% in step (4)³, excluding cavity mirror transmission. Additionally, we observed that intentionally displacing the right mirror by $\varepsilon_x \approx 100 \mu\text{m}$ reduced TEM₀₀ fiber-coupled power by 50%, generally consistent with the result in Fig. 3(a).

During step (5) we found the the coupling efficiency

dropped to 22% due to epoxy shrinkage during epoxy curing. We tried to compensate by adjusting the ferrule position but its response was sluggish after the epoxy became viscous. We anticipate that greater vigilance and active alignment during curing will avoid this problem. Figure 4(b) shows the ferrule potted inside the holder and the appearance of the completed assembly.

IV. CONCLUSION AND FUTURE

We analyzed the impact of various misalignments on coupling a FP TEM₀₀ mode to a single-mode fiber using a metalens. Our sensitivity and coupling efficiency calculations reveal that transverse misalignment is more critical than longitudinal ones. Our work complements recent atom-cavity coupling analysis [16]. We then built and tested a compact monolithic assembly. While the final coupling efficiency was limited, the 94% relative fiber coupling efficiency in step (4) is representative of the excellent performance metamaterial optics.

BIBLIOGRAPHY

-
- [1] C. Robens, S. Brakhane, W. Alt, F. Kleiβler, D. Meschede, G. Moon, G. Ramola, and A. Alberti, *Opt. Lett.* **42**, 1043 (2017).
- [2] A. Cooper, J. P. Covey, I. S. Madjarov, S. G. Porsev, M. S. Safronova, and M. Endres, *Phys. Rev. X* **8**, 041055 (2018).
- [3] A. Browaeys and T. Lahaye, *Nat. Phys.* **16**, 132 (2020).
- [4] R. He, J.-M. Cui, R.-R. Li, Z.-H. Qian, Y. Chen, M.-Z. Ai, Y.-F. Huang, C.-F. Li, and G.-C. Guo, *Review of Scientific Instruments* **92**, 073201 (2021).
- [5] A. L. Carter, J. O'Reilly, G. Toh, S. Saha, M. Shalaev, I. Goetting, and C. Monroe, *Review of Scientific Instruments* **95**, 033201 (2024).
- [6] S.-A. Guo, Y.-K. Wu, J. Ye, L. Zhang, W.-Q. Lian, R. Yao, Y. Wang, R.-Y. Yan, Y.-J. Yi, Y.-L. Xu, B.-W. Li, Y.-H. Hou, Y.-Z. Xu, W.-X. Guo, C. Zhang, B.-X. Qi, Z.-C. Zhou, L. He, and L.-M. Duan, *Nature* **630**, 613 (2024).
- [7] D. B. Bucher, D. P. L. Aude Craik, M. P. Backlund, M. J. Turner, O. Ben Dor, D. R. Glenn, and R. L. Walsworth, *Nat Protoc* **14**, 2707 (2019).
- [8] P. Senellart, G. Solomon, and A. White, *Nature Nanotech* **12**, 1026 (2017).
- [9] L.-M. Duan, M. D. Lukin, J. I. Cirac, and P. Zoller, *Nature* **414**, 413 (2001).
- [10] A. Reiserer and G. Rempe, *Rev. Mod. Phys.* **87**, 1379 (2015).
- [11] S. L. N. Hermans, M. Pompili, H. K. C. Beukers, S. Baier, J. Borregaard, and R. Hanson, *Nature* **605**, 663 (2022).
- [12] D. P. Nadlinger, P. Drmota, B. C. Nichol, G. Araneda, D. Main, R. Srinivas, D. M. Lucas, C. J. Ballance, K. Ivanov, E. Y.-Z. Tan, P. Sekatski, R. L. Urbanke, R. Renner, N. Sangouard, and J.-D. Bancal, *Nature* **607**, 682 (2022).
- [13] H. Takahashi, E. Kassa, C. Christoforou, and M. Keller, *Phys. Rev. Lett.* **124**, 013602 (2020).
- [14] M. Brekenfeld, D. Niemietz, J. D. Christesen, and G. Rempe, *Nature Physics* **16**, 647 (2020).
- [15] H. Goto, S. Mizukami, Y. Tokunaga, and T. Aoki, *Phys. Rev. A* **99**, 053843 (2019).
- [16] S. Gao, J. A. Blackmore, W. J. Hughes, T. H. Doherty, and J. F. Goodwin, *Phys. Rev. Appl.* **19**, 014033 (2023).
- [17] W. J. Hughes, T. H. Doherty, J. A. Blackmore, P. Horak, and J. F. Goodwin, *Opt. Express* **31**, 32619 (2023).
- [18] D. Hunger, T. Steinmetz, Y. Colombe, C. Deutsch, T. W. Hänsch, and J. Reichel, *New J. Phys.* **12**, 065038 (2010).
- [19] G. Rempe, R. J. Thompson, H. J. Kimble, and R. Lalezari, *OPTICS LETTERS* **17**, 3 (1992).
- [20] N. Jin, C. A. McLemore, D. Mason, J. P. Hendrie, Y. Luo, M. L. Kelleher, P. Kharel, F. Quinlan, S. A. Diddams, and P. T. Rakich, *Optica* **9**, 965 (2022).
- [21] J. Gallego, S. Ghosh, S. K. Alavi, W. Alt, M. Martinez-Dorantes, D. Meschede, and L. Ratschbacher, *Appl. Phys. B* **122**, 47 (2016).
- [22] A. Bick, C. Staarmann, P. Christoph, O. Hellmig, J. Heinze, K. Sengstock, and C. Becker, *Review of Scientific Instruments* **87**, 013102 (2016).
- [23] H. Pfeifer, L. Ratschbacher, J. Gallego, C. Saavedra, A. Faβbender, A. von Haaren, W. Alt, S. Hofferberth, M. Köhl, S. Linden, and D. Meschede, *Appl. Phys. B* **128**, 29 (2022).
- [24] G. K. Gulati, H. Takahashi, N. Podoliak, P. Horak, and M. Keller, *Sci Rep* **7**, 5556 (2017).

³ The relative fiber coupling efficiency excludes metalens transmission losses and refraction efficiency.

- [25] H.-T. Chen, A. J. Taylor, and N. Yu, *Rep. Prog. Phys.* **79**, 076401 (2016).
- [26] T. Phan, D. Sell, E. W. Wang, S. Doshay, K. Edee, J. Yang, and J. A. Fan, *Light Sci Appl* **8**, 48 (2019).
- [27] T.-W. Hsu, W. Zhu, T. Thiele, M. O. Brown, S. B. Papp, A. Agrawal, and C. A. Regal, *PRX Quantum* **3**, 030316 (2022).
- [28] R. Huang, F. Zhou, X. Li, P. Xu, Y. Wang, and M. Zhan, *Opt. Express* **32**, 21293 (2024).
- [29] G.-J. Chen, D. Zhao, Z.-B. Wang, Z. Li, J.-Z. Zhang, L. Chen, Y.-L. Zhang, X.-B. Xu, A.-P. Liu, C.-H. Dong, G.-C. Guo, K. Huang, and C.-L. Zou, *Laser & Photonics Reviews* **n/a**, 2401595 (2024).
- [30] H. Lim, J. Froech, M. Choi, A. Majumdar, and S. Mouradian, in *Quantum 2.0 Conference and Exhibition (2024)*, *Paper QM3A.3* (Optica Publishing Group, 2024) p. QM3A.3.
- [31] H. Ren, G. Briere, X. Fang, P. Ni, R. Sawant, S. Héron, S. Chenot, S. Vézian, B. Damilano, V. Brändli, S. A. Maier, and P. Genevet, *Nat Commun* **10**, 2986 (2019).
- [32] Q. Zhou, M. Liu, W. Zhu, L. Chen, Y. Ren, H. J. Lezec, Y. Lu, A. Agrawal, and T. Xu, *Laser & Photonics Reviews* **15**, 2100390 (2021).
- [33] M. Osslander, M. L. Meretska, S. Rourke, C. Spägele, X. Yin, I.-C. Benea-Chelmus, and F. Capasso, *Nat Commun* **14**, 1114 (2023).
- [34] Y. Fontana, R. Zifkin, E. Janitz, C. D. Rodríguez Rosenblueth, and L. Childress, *Review of Scientific Instruments* **92**, 053906 (2021).
- [35] O. Wipfli, H. F. Passagem, C. Fischer, M. Grau, and J. P. Home, *Review of Scientific Instruments* **94**, 083204 (2023).
- [36] A. Kumar, A. Suleymanzade, M. Stone, L. Taneja, A. Anferov, D. I. Schuster, and J. Simon, *Nature* **615**, 614 (2023).
- [37] C. H. Nguyen, A. N. Utama, N. Lewty, and C. Kurtsiefer, *Phys. Rev. A* **98**, 063833 (2018).
- [38] V. Krutyanskiy, M. Canteri, M. Meraner, J. Bate, V. Krčmánský, J. Schupp, N. Sangouard, and B. P. Lanyon, *Phys. Rev. Lett.* **130**, 213601 (2023).
- [39] A. Periwal, E. S. Cooper, P. Kunkel, J. F. Wienand, E. J. Davis, and M. Schleier-Smith, *Nature* **600**, 630 (2021).
- [40] E. Deist, Y.-H. Lu, J. Ho, M. K. Pasha, J. Zeiher, Z. Yan, and D. M. Stamper-Kurn, *Phys. Rev. Lett.* **129**, 203602 (2022).
- [41] D. Shadmany, A. Kumar, A. Soper, L. Palm, C. Yin, H. Ando, B. Li, L. Taneja, M. Jaffe, S. David, and J. Simon, *Science Advances* **11**, eads8171 (2025).
- [42] Corning, SMF-28 Ultra Optical Fibers | SMF-28 Ultra 200 and 242 Mm Single-mode Optical Fiber | Corning, <https://www.corning.com/optical-communications/worldwide/en/home/products/fiber/optical-fiber-products/smf-28-ultra.html> (2024).
- [43] W. B. Joyce and B. C. DeLoach, *Appl. Opt.* **23**, 4187 (1984).
- [44] Products or companies named here are included in the interest of completeness and does not imply endorsement by the authors.
- [45] V. Egede Johansen, U. M. Gür, J. Martínez-Llinás, J. Fly Hansen, A. Samadi, M. Skak Vestergaard Larsen, T. Nielsen, F. Mattinson, M. Schmidlin, N. A. Mortensen, and U. J. Quaade, *Commun Phys* **7**, 1 (2024).
- [46] Norland, NOA 61 | Norland Products, Inc., <https://norlandproducts.com/product/nea-61/> (2024).
- [47] Masterbond, EP42HT-3AO Product Information | MasterBond.com, <https://www.masterbond.com/tds/ep42ht-3ao> (2024).
- [48] C. S. Adams, J. D. Pritchard, and J. P. Shaffer, *J. Phys. B: At. Mol. Opt. Phys.* **53**, 012002 (2019).
- [49] G. Aranedá, G. Cerchiari, D. B. Higginbottom, P. C. Holz, K. Lakhmanskiy, P. Obšil, Y. Colombe, and R. Blatt, *Review of Scientific Instruments* **91**, 113201 (2020).
- [50] K. Bergmann, H.-C. Nägerl, C. Panda, G. Gabrielse, E. Miloglyadov, M. Quack, G. Seyfang, G. Wichmann, S. Ospelkaus, A. Kuhn, S. Longhi, A. Szameit, P. Pirro, B. Hillebrands, X.-F. Zhu, J. Zhu, M. Drewsen, W. K. Hensinger, S. Weidt, T. Halfmann, H.-L. Wang, G. S. Paroanu, N. V. Vitanov, J. Mompart, T. Busch, T. J. Barnum, D. D. Grimes, R. W. Field, M. G. Raizen, E. Narevicius, M. Auzinsh, D. Budker, A. Pálffy, and C. H. Keitel, *J. Phys. B: At. Mol. Opt. Phys.* **52**, 202001 (2019).
- [51] M. Ghadimi, V. Blüms, B. G. Norton, P. M. Fisher, S. C. Connell, J. M. Amini, C. Volin, H. Hayden, C.-S. Pai, D. Kielpinski, M. Lobino, and E. W. Streed, *npj Quantum Inf* **3**, 1 (2017).
- [52] R. Juliano Martins, E. Marinov, M. A. B. Youssef, C. Kyrou, M. Joubert, C. Colmagro, V. Gâté, C. Turbil, P.-M. Coulon, D. Turover, S. Khadir, M. Giudici, C. Klitis, M. Sorel, and P. Genevet, *Nat Commun* **13**, 5724 (2022).
- [53] E. Kassa, *Single Ion Coupled to a High-Finesse Optical Fibre Cavity for cQED in the Strong Coupling Regime*, Doctoral, University of Sussex (2017).
- [54] R. Noek, G. Vrijsen, D. Gaultney, E. Mount, T. Kim, P. Maunz, and J. Kim, *Opt. Lett.* **38**, 4735 (2013).
- [55] D. B. Northeast, D. Dalacu, J. F. Weber, J. Phoenix, J. Lapointe, G. C. Aers, P. J. Poole, and R. L. Williams, *Sci Rep* **11**, 22878 (2021).
- [56] J.-S. Park, S. Zhang, A. She, W. T. Chen, P. Lin, K. M. A. Yousef, J.-X. Cheng, and F. Capasso, *Nano Lett.* **19**, 8673 (2019).
- [57] T. Ruelle, D. Jaeger, F. Fogliano, F. Braakman, and M. Poggio, *Review of Scientific Instruments* **93**, 095003 (2022).
- [58] C. Shen, C. Chen, X.-L. Wu, S. Dong, Y. Cui, L. You, and M. K. Tey, *Review of Scientific Instruments* **91**, 063202 (2020).
- [59] L. Stephenson, *Entanglement between Nodes of a Quantum Network*, <http://purl.org/dc/dcmitype/Text>, University of Oxford (2019).
- [60] L. J. Stephenson, D. P. Nadlinger, B. C. Nichol, S. An, P. Drmota, T. G. Ballance, K. Thirumalai, J. F. Goodwin, D. M. Lucas, and C. J. Ballance, *Phys. Rev. Lett.* **124**, 110501 (2020).
- [61] W. Wang, C. Goham, A. Laugharn, and J. W. Britton, in *OSA Quantum 2.0 Conference (2020)*, *Paper QW6A.12* (Optica Publishing Group, 2020) p. QW6A.12.
- [62] Y. Xiao, Z. Wang, F. Wang, H. Lee, T. Kananen, and T. Gu, *JOM* **1**, 024001 (2021).
- [63] C. B. Young, A. Safari, P. Huft, J. Zhang, E. Oh, R. Chinnarasu, and M. Saffman, *Appl. Phys. B* **128**, 151 (2022).